A Comparison Between a Non-Linear and a Linear Gaussian Statistical Detector for Detecting Dim Satellites

Lt Stephen Maksim
United States Air Force
Maj J. Chris Zingarelli
United States Air Force
Dr. Stephen Cain
Air Force Institute of Technology

ABSTRACT

This paper describes and analyzes a Gaussian statistical satellite detection algorithm. This detection algorithm exploits the correlation of pixels that arises from the long-term exposure point spread function (PSF) due to diffraction and atmospheric effects. This correlating detection algorithm is compared to a simple, linear threshold detection algorithm, which treats the probability density function (PDF) of the photons as Gaussian and the PSF as Dirac. The effects of changing the window size and grid size is explored and analyzed. Using a dataset collected by the Space Surveillance Telescope (SST) that shows many samples of a geostationary satellite gradually going into eclipse during the vernal equinox, the probabilities of detection for the algorithms are compared as the satellite becomes very dim and nearly disappears to determine which detection algorithm performs better. A better performing detection algorithm will allow detection of satellites, space debris, and other dim objects that have not been visible before.

1. INTRODUCTION

This paper investigates what gains can be achieved by using a non-linear log-likelihood detector that exploits the correlation that results from diffraction over current techniques that only consider the light from a single pixel. It also analyzes the effects of changing the size of both the window and the search grid on the performance of both algorithms. First the experiment that provided data for this analysis is introduced. Then a mathematical Gaussian detection algorithm is provided, followed by a discussion of the methodology and limitations of the comparison. Finally the results are discussed and analyzed. That correlation provides a better probability of detection is expected. Without an understanding of the conditions under which both the single point and the correlated detectors work best, though, it is difficult to determine whether either is being implemented wisely in a given situation.

2. EXPERIMENT

The goal of this research project is to compare the performance of detection algorithms under very low light conditions. A glint experiment done by the USNO (United States Naval Observatory) this past fall served as the blueprint for the experiment that we conducted [1]. In their experiment, a geostationary satellite was imaged going into eclipse during the autumnal equinox. Data from the USNO in table 1 shows how a rapid series of images revealed the satellite growing dimmer gradually until it disappears entirely. This situation presents the observer with an object whose intensity is varying in time, which allows detection algorithms to be tested over a variety of light levels. Also because the object can be clearly observed heading into the eclipse, its position is relatively well known throughout the experiment. These attributes make this type of test ideal for comparing the performance of different detection algorithms.

Report Documentation Page	*Form Approved* *OMB No. 0704-0188*

1. REPORT DATE **SEP 2012**	2. REPORT TYPE	3. DATES COVERED **00-00-2012 to 00-00-2012**
4. TITLE AND SUBTITLE **A Comparison Between a Non-Linear and a Linear Gaussian Statistical Detector for Detecting Dim Satellites**		5a. CONTRACT NUMBER
		5b. GRANT NUMBER
		5c. PROGRAM ELEMENT NUMBER
6. AUTHOR(S)		5d. PROJECT NUMBER
		5e. TASK NUMBER
		5f. WORK UNIT NUMBER
7. PERFORMING ORGANIZATION NAME(S) AND ADDRESS(ES) **United States Air Force,Washington,DC,20301**		8. PERFORMING ORGANIZATION REPORT NUMBER
9. SPONSORING/MONITORING AGENCY NAME(S) AND ADDRESS(ES)		10. SPONSOR/MONITOR'S ACRONYM(S)
		11. SPONSOR/MONITOR'S REPORT NUMBER(S)

12. DISTRIBUTION/AVAILABILITY STATEMENT
Approved for public release; distribution unlimited

13. SUPPLEMENTARY NOTES
Presented at the 13th annual Advanced Maui Optical and Space Surveillance (AMOS) Technologies Conference on September 11-14, 2012 Maui, Hawai

14. ABSTRACT
This paper describes and analyzes a Gaussian statistical satellite detection algorithm. This detection algorithm exploits the correlation of pixels that arises from the long-term exposure point spread function (PSF) due to diffraction and atmospheric effects. This correlating detection algorithm is compared to a simple, linear threshold detection algorithm, which treats the probability density function (PDF) of the photons as Gaussian and the PSF as Dirac. The effects of changing the window size and grid size is explored and analyzed. Using a dataset collected by the Space Surveillance Telescope (SST) that shows many samples of a geostationary satellite gradually going into eclipse during the vernal equinox, the probabilities of detection for the algorithms are compared as the satellite becomes very dim and nearly disappears to determine which detection algorithm performs better. A better performing detection algorithm will allow detection of satellites, space debris, and other dim objects that have not been visible before.

15. SUBJECT TERMS

16. SECURITY CLASSIFICATION OF:			17. LIMITATION OF ABSTRACT	18. NUMBER OF PAGES	19a. NAME OF RESPONSIBLE PERSON
a. REPORT **unclassified**	b. ABSTRACT **unclassified**	c. THIS PAGE **unclassified**	**Same as Report (SAR)**	**9**	

Table 1. Digital counts for Anik F1 entering the terminator during autumnal equinox. Provided by Dave Monet, USNO

From USNO Telescope w/Orthogonal Transfer CCD*		
Frame	UT	Counts above sky
2500	25:31.1	saturation
2550	40:41.1	7100
2560	41:31.0	2000
2570	42:21.2	1100
2580	43:11.2	700
2590	44:01.3	400
2600	44:51.2	200
2610	45:41.2	200
2620	46:31.4	200
2630	47:21.4	150
2640	48:11.2	50
2650	49:01.3	0

In our experiment the recently-constructed SST telescope imaged a geostationary communications satellite as it went in and out of eclipse for eleven nights between 28 February and 23 March 2012 during the vernal equinox. We also imaged Anik F1, which flies at 107.3º W longitude and is 40.4 x 9 meters at its largest dimensions. The satellite was actively tracked from its orbital elements through the entire eclipse. The result is a dataset in which a very dim object is in a known location, providing the opportunity to test detection algorithms under a wide variety of light conditions. Since the satellite was tracked, other objects in the sky pass through at the sidereal rate. Pictures were taken every five seconds, resulting in relatively gradual changes between frames. Both binned (2x2) and un-binned pixel data was collected, but only binned data is included in this analysis.

The dataset does not provide a basis for forming receiver operating characteristic (ROC) curves. The design of SST is unprecedented, and it is certainly capable of seeing things that have not been seen before. Thus, it is extremely difficult to assert that it is imaging a blank sky, which is the necessary condition for computing the probability of false alarm.

3. GAUSSIAN LOG-LIKELIHOOD DETECTORS

3.1 Mathematical Basis
The satellite is considered to be present in a pixel $d(x, y)$ in the image when the likelihood ratio, Λ, exceeds a threshold, η, as in:

$$\Lambda(x, y) = \frac{P\left[d(w, z) \mid H_1\right]}{P\left[d(w, z) \mid H_0\right]} \overset{H_1}{\underset{H_0}{\gtrless}} \eta$$

The model that assumes that the noise in the image is Gaussian is considered first. The probabilities that the object is present (H_1) or not (H_0) are:

$$P\left[d(w,z)\mid H_1\right] = \prod_w^N \prod_z^N \frac{1}{\sqrt{2\pi}\sigma}\, e^{\left\{-\frac{1}{2\sigma^2}\left[d(w,z)-B-\theta\otimes h\right]^2\right\}}$$

and

$$P\left[d(w,z)\mid H_0\right] = \prod_w^N \prod_z^N \frac{1}{\sqrt{2\pi}\sigma}\, e^{\left\{-\frac{1}{2\sigma^2}\left[d(w,z)-B\right]^2\right\}}$$

where $d(w,z)$ are pixels in a square $N\times N$ window of the image centered on $d(x,y)$, B is the expected value of the background of the window, σ is the standard deviation of the background of the window, θ is a scale factor for the expected amount of light, and h is the point spread function of the system. Whereas analysis of data from other experiments like the Panoramic Survey Telescope & Rapid Response System (Pan-Starrs) is able to make use of foreknowledge of the background, the background is approximated in this comparison by the mean of the image in the window:

$$B = \sum_w^N \sum_z^N \frac{d(w,z)}{N^2}$$

This is a good approximation when the window size is chosen to include the tails of the PSF (point spread function) so that the intensity of most of the pixels in the window is dominated by the background.

Likewise, σ, the standard deviation of the background, is given by:

$$\sigma(x,y) = \sqrt{\frac{\sum_w^N \sum_z^N d^2(w,z)}{N^2} - \left(\frac{\sum_w^N \sum_z^N d(w,z)}{N^2}\right)^2}$$

Taking the natural log changes the products to summations, allows the removal of constants and a lower dynamic range of equation [2]. Simplifying, the result is:

$$\ln\Lambda(x,y) = \sum_w^N \sum_z^N \frac{(d(w,z)-B)h(w,z)}{\sigma} \underset{H_0}{\overset{H_1}{\underset{<}{>}}} \eta$$

Since $d(w,z)$ is assumed to be Gaussian, then when the background is subtracted and that sum is divided by the standard deviation, the result is a normal Gaussian variable, with zero mean and unit variance. [1]

3.2 Transfer Functions

Examining only the center pixel with coordinates (c_x, c_y) and ignoring correlation in the rest of the image is equivalent to treating the transfer function of the system as a Dirac delta function. Accordingly, we can use the sifting property of the Dirac to make the following simplification for the Gaussian-Dirac detector:

$$\ln\Lambda(c_x, c_y) = \sum_w^N \sum_z^N \frac{(d(w,z)-B)h_\delta(c_x, c_y)}{\sigma} = \sum_w^N \sum_z^N \frac{(d(w,z)-B)\delta(w-c_x, z-c_y)}{\sigma} = \frac{(d(c_x, c_y)-B)}{\sigma}$$

In contrast, correlation in the image can be included by using the PSF as the transfer function of the system. Thus, the Gaussian-PSF detector considers the correlation of all the pixels in the window:

$$\ln \Lambda(c_x, c_y) = \sum_w^N \sum_z^N \frac{(d(w,z) - B)h_{PSF}(w + c_x, z + c_y)}{\sigma}$$

4. METHODOLOGY

4.1 Determination of the PSF

The normalized PSF of the satellite for a given eclipse event is derived from $\overline{d}_{PSF}(x, y)$, an average of the first ten frames after the satellite stops glinting

$$\overline{d}_{PSF}(x, y) = \sum_{frame=1}^{10} \frac{d_{frame}(x, y)}{10}$$

where $d(x, y)$ are images of the satellite and (x, y) are elements of an $N \times N$ window centered on the satellite. The normalized PSF is computed by

$$PSF(x, y) = \frac{\overline{d}_{PSF}(x, y) - \min(\overline{d}_{PSF})}{\sum_x^N \sum_y^N (\overline{d}_{PSF}(x, y) - \min(\overline{d}_{PSF}))}$$

Subtracting $\min(\overline{d}_{PSF})$, which is the lowest value found in $\overline{d}_{PSF}(x, y)$, removes as much of the background as possible while preserving the tails of the PSF. Foreknowledge of the PSF of the satellite certainly helps in detection. Essentially, it helps to know what it is that one is looking for, and there are many cases in which one does have an opportunity to image an object before subsequently searching for it. A generalized PSF could also be used that was based on: the parameters of the telescope used; the long exposure OTF (optical transfer function) of the atmosphere; and the general knowledge of the size and shape of the object being looked for.

4.2 Search Pattern and Logic

The image of the satellite moves perceptibly from frame to frame. Reasons for this include atmospheric diffraction (mainly tilt aberrations), errors in tracking, orbital path, and changes in how the light is reflected. Therefore, the algorithms are tried on all the pixels in a square search grid that is roughly centered on the satellite. The satellite is considered to be detected when it is found in any pixel in the search grid, the equivalent of applying a logical "or."

For the purposes of this analysis, the eclipse is considered to last from the first non-saturated frame to the last non-saturated frame. The algorithm was only used to detect objects during this defined eclipse period for a couple of reasons. First, the objects are easily detectable in saturated frames by simply searching for pixels that have an intensity that equals the maximum value of the ADC, so it is a trivial case. Second, at saturation charge spillover into nearby pixels distorts the data and saturation is in itself a significant non-linearity, both of which challenge the assumption that the system as a whole is essentially linear.

The threshold η is set to six for both algorithms, so that they are competing on an even basis. This was chosen because LINEAR (Licoln Near-Earch Asteroid Research) has been employing a threshold of $\eta = 6$ in their work [3]. For the purposes of comparison, the relative intensity $b(x, y)$ of a given point approximates the intensity of the noiseless signal and is defined as

$$b(x, y) = d(x, y) - B(x, y)$$

where $d(x, y)$ is the intensity of pixel and $B(x, y)$ is the background at that same point, as defined previously.

5. LIMITATIONS

To simplify the calculations, the windows used to compute statistics and to contain the PSF are square, even though the diffracted image is better approximated as a circle. If the window size is chosen well, then this effect should be minimized since the tails of the sinc function, which well describes diffraction [4], fall off quickly. However, any square window will have too much noise in the corners and not enough of the tail along the side.

If the window size is too large or small relative to the size of the object present, then the statistical detector cannot distinguish the object from the background. This problem is especially notable with the Gaussian-Dirac detector. For example, when using a 33-pixel wide window to process a 5 by 5 grid centered on the satellite right before the beginning of the eclipse on the night of 2 March, 2012 the Gaussian-Dirac detector does not detect the satellite at all until the 264th frame, whereas the Gaussian-PSF detector finds the satellite from the very first frame; the first non-saturated image is frame 281.

6. RESULTS

The total number of detections for the two competing algorithms on five nights is shown in fig. 1. Odd window sizes between 1 and 49 were tried. The results of different search grid sizes are shown for 2 Mar 2012. In terms of total detections, the Gaussian-Dirac never performed as well as the Gaussian-PSF. Frame by frame results are shown in fig. 2 for each of the tests. The character of 2 Mar 2012 is clearly different from the other nights, as the satellite seems especially apparent to the Gaussian-PSF detector long after it disappears from the Gaussian-Dirac detector. Some of the detections that are well after the eclipse has begun seem to be due to star crossings, but others seem legitimate; for most of those late detections it is difficult to say whether a dim star is present in the background or whether the satellite is truly detected.

The rapidity with which the satellite enters the eclipse changes from night to night. In an attempt to normalize for this difference, it is useful to examine the relative intensity $b(x, y)$ of the data for detections near the transition into total eclipse, after which the satellite seems to be essentially undetectable. The selection of these points was done by hand by choosing the successful detection near the end that seemed to have the lowest light level. For the night of 2 Mar 2012, frame 500 was the last frame with a detection by the Gaussian-Dirac algorithm, and 532 was the last frame with a detection by the Gaussian-PSF algorithm. These frames were examined to determine which pixels registered the detection, and $b(x, y)$ was computed for those pixels. The minimum of these pixels for a given frame is represented by b-psf for the Gaussian-PSF and b-Dirac for the Gaussian-Dirac. In computing the background B for use in finding $b(x, y)$ for each frame and algorithm, the window size that detected the most frames in that dataset was used (the maximum value for each algorithm in fig. 1).

The ratio of their intensities was found to be

$$\left| \frac{b_{PSF}(x, y)}{b_{Dirac}(x, y)} \right| = 0.374$$

which can be interpreted to mean that the Gaussian-PSF detector found the satellite when it was only about a third as bright.

For the night of 14 Mar 2012, frames 834 and 854 were selected for the Gaussian-Dirac and Gaussian-PSF detectors, respectively; although 834 was not the last frame, it was certainly the frame with the lowest light in the adjacent area. The ratio of their intensities was found to be:

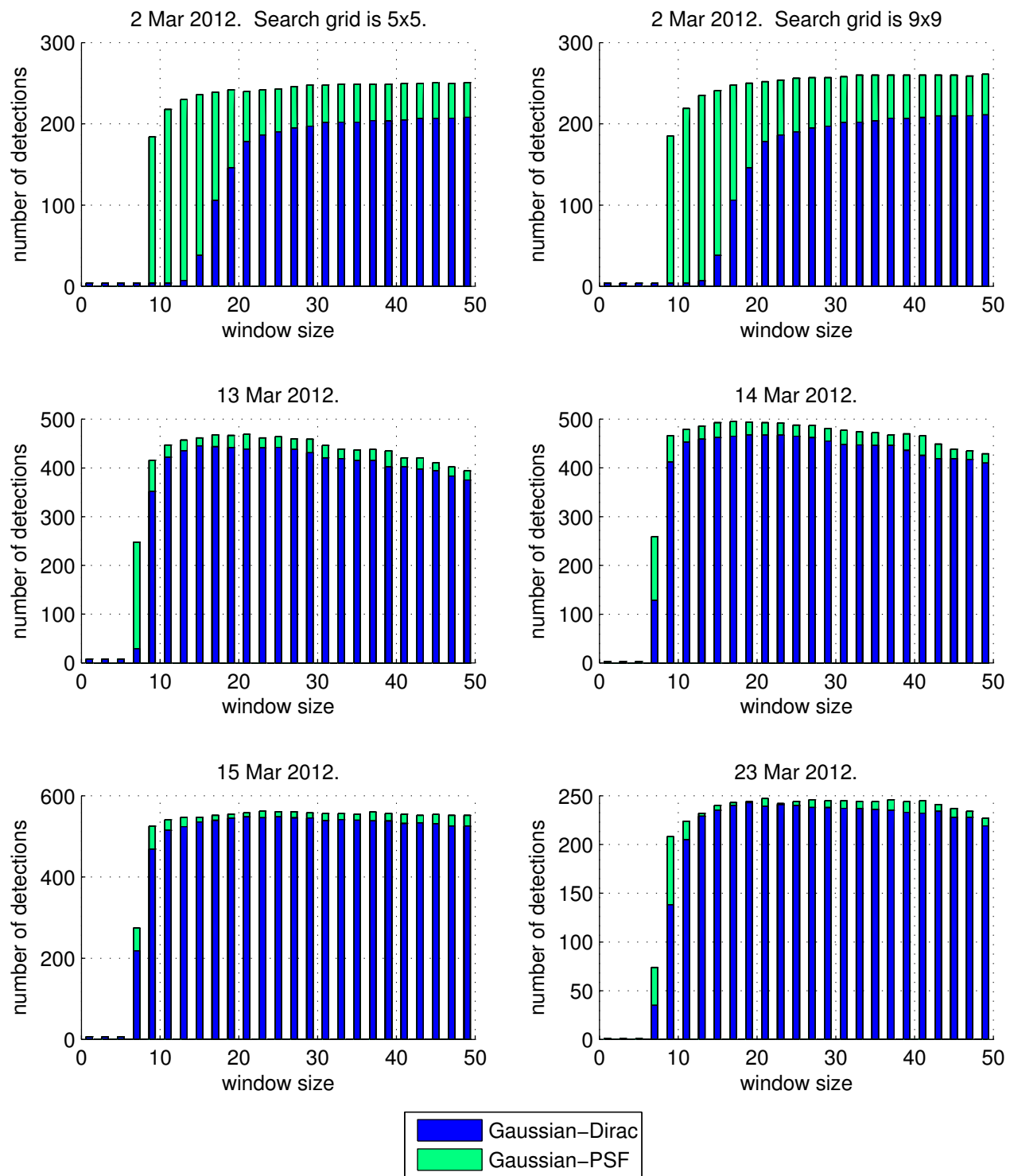$$\left| \frac{b_{PSF}(x, y)}{b_{Dirac}(x, y)} \right| = 0.02$$

Fig. 1. Comparison of the number of detections for both algorithms. The Gaussian-Dirac is shown in blue in front. The Gaussian-PSF is shown in green and is behind the Gaussian-Dirac. The algorithms were computed using odd window sizes between 1 and 49 on each of the different nights. The search grid is 9x9, unless otherwise noted.
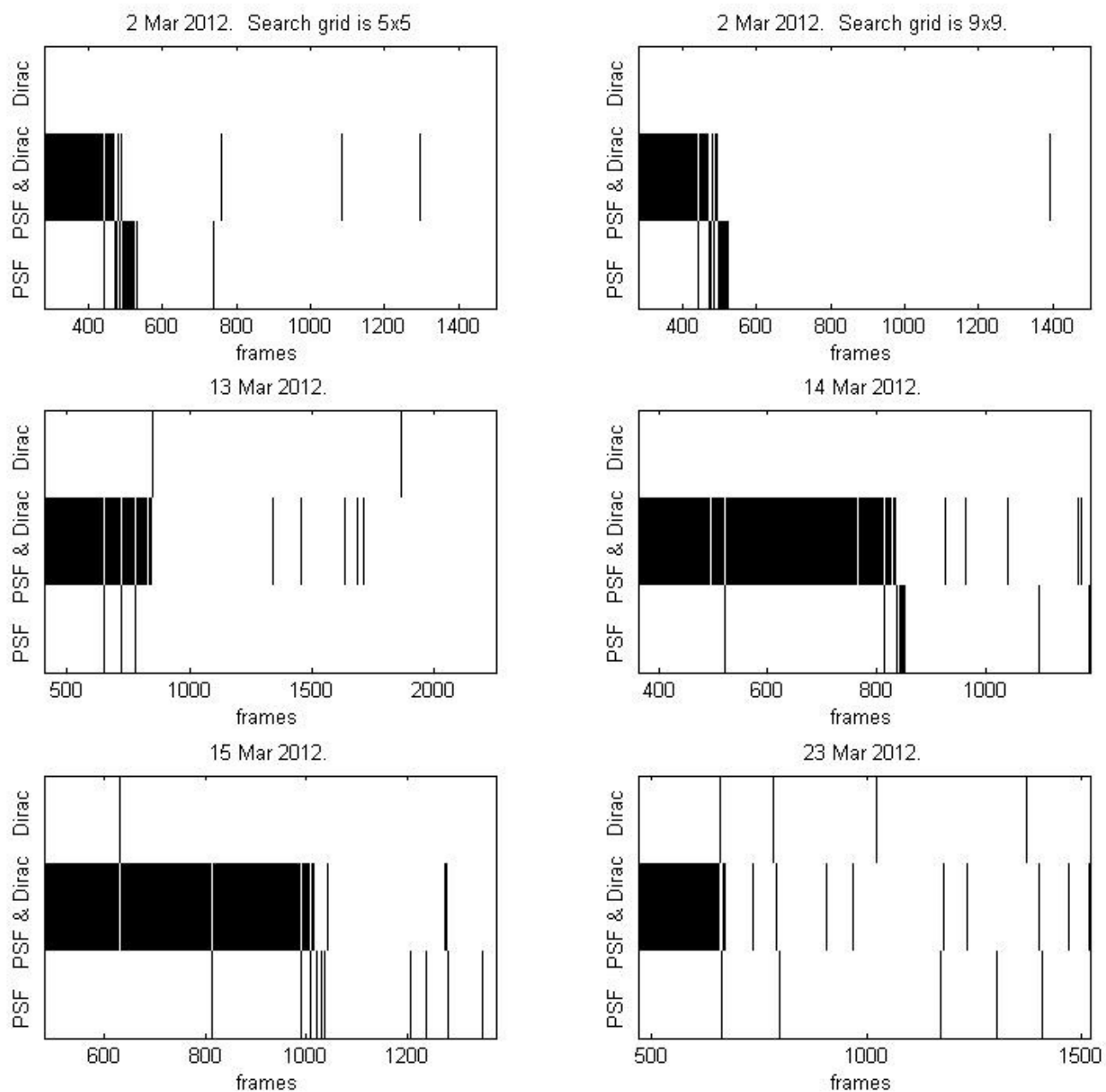
Fig. 2. Detections of the satellite, frame by frame, for the window size that yielded the most detections according to the total number, bounded by 49x49. If multiple window sizes were equally effective, the smallest was used. The upper third shows frames that only the Gaussian-Dirac algorithm detected the satellite. The middle third shows frames that both the Gaussian-Dirac and the Gaussian-PSF algorithms detected the satellite. The lower third shows frames that only the Gaussian-PSF algorithm detected the satellite. The search grid was 9x9, unless otherwise noted. The initial frame is the first non-saturated frame.

7. ANALYSIS

Past a certain minimum, the size of the window has a relatively small impact on the results, especially in proportion to the additional computational requirements. This shelving is reached more quickly and is more pronounced for the Gaussian-PSF detector than it is for the Gaussian-Dirac detector. The best explanation for the difference in the results for 2 Mar 2012 from the other nights seems to be that for whatever reason the satellite seemed to pass more slowly into the terminator on 2 Mar 2012. Though that night does seem to be a bit of an outlier, the smoothness of its curves in fig. 1 lend credence to the data.

The curves in Fig. 1 also suggest that the ideal window size for both algorithms is in the upper teens or low twenties. Though some of the highest detections were above this range, they were not dependably; the total number of detections actually declined as the window size approached 49x49 for three and four of the nights with the Gaussian-PSF and Gaussian-Dirac algorithms, respectively. Also, neglecting efficiencies that can be found with vector processing, the computational cost of computing either algorithm increases roughly proportional to the area of the window, N^2.

As can be seen in fig. 2, the Gaussian-Dirac algorithm does register an appreciable amount of detections that the Gaussian-PSF algorithm does not. If forced to choose only one, the Gaussian-PSF might yield better results; however, the best option might be to choose both. If the same window size is used for both algorithms, then the computational burden is significantly lower since the window is already in memory and the mean has been computed.

8. CONCLUSION

This paper has compared the Gaussian-Dirac and the Gaussian-PSF log-likelihood detection algorithms and shown how search grid size and window size affect their performance in detecting a satellite in varying degrees of illumination. The Gaussian-PSF performed better, as was expected. This study should help in selecting the optimal parameters, whichever algorithm is used in the detection of dim objects.

9. ACKNOWLEDGEMENTS

10. REFERENCES

1.   Vrba, Frederick J., et al., A Survey of Geosynchronous Satellite Glints, Proceedings 2009 AMOS Technical Conference, 2009.
2   Richmond, Richard D. and Cain, Stephen C., *Direct-Detection LADAR Systems,* SPIE Press, Bellingham, Washington, 2010.
3   Pearce, E.C., et al., High Precision Real Time Metric Processing for the MOSS and LINEAR Systems, Proceedings of the 2000 Space Control Conference, 145-157, 2000.
4   Goodman, Joseph W., *Introduction to Fourier Optics*, Roberts & Company Publishers, Greenwood Village, Colorado, 2005.